Energy Modeling Based on Power Profiling of Wireless Sensor Device

Rivo Randriatsiferana, Frederic Alicalapa, Richard Lorion, Lala Rajaoarisoa, Blaise Ravelo, Christophe Moy

Energy Modelling Based On Power Profiling of Wireless Sensor Device

Rivo Randriatsiferana, Frédéric Alicalapa, Richard Lorion, Lala Rajaoarisoa, Blaise Ravelo and Christophe Moy

Abstract— **This paper elaborates an accurate energy model for Wireless Sensor Device (WSD) based on power consumption measurement. A deep understanding of WSD's energy cost depends on the WSD's functional components contributing to the wireless communication process. The model includes different stages of transmission and reception communication modes. The practical energy model (EM) is developed with data packet lengths, data rate, operation status, pre-designed stages versus appropriate communication bus and power mode including mutual data transfers between the microcontroller and the radio module. The validity of the EM is verified through an experimental setup having a TelosB device. As expected, the modelled and measured energy consumed by the WSD operating from 1-to-4-MHz CPU frequency and 2-to-100 Bytes payload are in very good agreement. It was found that compared to the energy consumption in processing, transmission, listening and reception phases, the data transfer consumes up to 40% of total WSD energy whereas this aspect is often neglected in usual models. Overall, the proposed model provides significant accuracy and might be helpful in improving the energy efficiency of future wireless sensor networks.**

Index Terms— **WSN, Communication process, Power measurement, Power profiling, Energy evaluation, Energy modelling.**

I. INTRODUCTION

TO SATISFY the public and industrial needs, the wireless sensor networks (WSNs) used for the internet of things must operate under the challenge of lifetime maximization [1]–[3]. WSNs are interconnected by wireless sensor devices (WSDs) that are densely deployed for gathering data about the surrounding environment [1]. The WSDs consist of miniature embedded systems with limited resources, like microcontroller (MCU) capacity, radio communication range, and the battery-powered energy [3]–[5]. The energy and resource management constraints become essentially an operational nature and expected features for WSN design methodologies [5]. Indeed, to achieve an acceptable network lifetime, the energy consumption issue must be addressed across the WSN design level.

Many research works were focused on energy sobriety and

R. Randriatsiferana and C. Moy are with the Univ Rennes, CNRS, IETR-UMR 6164, F-35000 Rennes, France (e-mail: rivo.randriatsiferana@univ-rennes1.fr, christophe.moy@univ-rennes1.fr).

F. Alicalapa and R. Lorion are with University of La Reunion, Energy Lab, 97400 La Reunion, France (e-mail: frederic.alicalapa@univ-reunion.fr, richard.lorion@univ-reunion.fr).

L. Rajaoarisoa is with the IMT Nord Europe, University of Lille, Centre for Digital Systems, F-59000 Lille, France (e-mail: lala.rajaoarisoa@imt-nord-europe.fr).

B. Ravelo is with Nanjing University of Information and Science Technology, Nanjing, Jiangsu 210044, China (e-mail:blaise.ravelo@yahoo.fr).

energy efficiency of the WSN considering different aspects such as WSD platforms [3]–[5], device subsystems architecture [6]–[12], communication protocols [13]–[22], network architecture organization [23]–[26], and routing techniques [27]–[31]. Alternative works have attempted to develop WSDs placement strategy for reducing the energy hole problem [32]–[34], and to alleviate the time synchronization issue [35]. Furthermore, many works have addressed the design of real-time operating systems [36]–[39]. They tackle the WSD resource constraints generally, by including limited memory which often allows storing only some kilobytes, and limited power such that the MCU-unit runs in low power mode (LPM) to save energy. Despite these energy-saving techniques, the real-time assessment of the WSN device remains an open-challenge for a system designer.

The major difficulty in carrying out a proper analysis of the WSN lifetime arises because of the non-availability of accurate energy models. An inaccurate energy model (EM) leads to an inaccurate network lifetime estimation [40]. This challenge gets further tightened because of the time-dependent nature of the energy consumption model [9]–[15]. Over the past two decades, many modelling methods have been proposed for evaluating WSN performances. Based on the objectives of the WSN design, the energy modelling methods follow either theoretical or practical approaches. Moreover, they rely on the assumption that the radio module (RM) is the most energy-consuming module in WSDs [4]–[6].

The analytical-based radio EM was proposed to estimate the energy needed to send and receive the data packet. This model is often used to evaluate the routing techniques, and network architecture organization in terms of both the energy efficiency and the network lifetime [1]–[3]. In this EM, the energy consumption of processing, reception (Rx) and transmission (Tx) electronic circuit have been assumed to be constant, and the Tx output power is assumed to be varying. The Tx output power is expressed as a function of the distance between the transmitter and receiver, which in turn depends on the free-space and multipath fading channel models [23]–[31]. Other works have proposed energy models to alleviate the energy cost optimization issues. These works consider individual sub-systems that constitute the RM circuit chains. For instance, the baseband subsystem, modulation or demodulation (Modem), power amplifier (PA), intermediate-frequency amplifier (IFA), low noise amplifier (LNA), frequency synthesizer (FS) and voltage controlled oscillator (VCO) [6]–[12].

A practical energy model is derived from device measurement results which take into consideration energy dissipation of each of the circuit components at the physical (PHY) layer [13]–[15]. This model is often used to evaluate the energy sobriety of the communication protocols in terms of the energy-saving and the network lifetime [16]–[22]. Also, these papers show that some system parameters such as data rate, operating frequency, and output power have a significant effect on the lifetime of the WSD. Moreover, it has been proved that the total consumed energy in the entire WSD lifetime depends significantly on the state of operation of the WSD, rather than on the energy consumption of both the data Tx and Rx module [15]. Actually, the RM is usually supposed to exist in steady states i.e., Rx, Tx, listening, off and sleeping, as well as all the transitions between these different states [41]–[43]. While the MCU has a low power management system, it can be into active, sleep and off states and the corresponding transition states [44]–[47]. However, the experiment realised in [43] noted a considerable difference, up to 20%, in overall energy consumption between simulation and practical results. We wish to assert that this happens because the proposed solutions do not consider modelling the energy consumed by the entire WSD.

Combining these different energy models into a holistic one and filling in the missing parts is not consistent, since these works have been proposed under different assumptions. The main reason is that the developed models study the MCU and the RM independently. Thus, the mutual interactions between the MCU and the RM are neglected when designing the energy model, disregarding the communication process. The profile of the power consumed by the WSDs allows a better understanding of its energy consumption in different states. The motivation of this work is to develop an accurate energy model that is supported by in situ power consumption measurements. The main objective is to obtain an adequate prediction of the WSD lifetime during the communication process. The contributions of this paper consist of:

- developing a novel practical-based energy model for a WSN based on an IEEE802.15.4 platform [4], which is time-dependent. The proposed timing diagram of the

WSD operation enables to identify all the state changes of the MCU and RM related to the communication process (Fig. 2). This diagram provides an accurate representation of the WSD behaviour and a fine prediction of its energy consumption. The proposed model supports variable payload size and depends on the physical layer parameters especially the data rate, power modes, operation frequency, and the predesigned stages versus appropriate communication bus, one of the characteristics was missing in the previous works. It allows for more accurate power consumption profile for all payload sizes.

- conducting new experimental measurements based on telosB device [48] following the bottom-up approach. As the WSD is supposed to run on battery power, it is important to know which part of the WSD draws the most power. We provide an accurate power consumption profile describing the different internal phases of the WSD under communication. The measurement results are used to verify the model precision by comparing the data sheet values with the measured values. The experimental validation demonstrates the model accuracy for all payload sizes from 2-to-100 bytes, and the calculated power consumption differs on average by less than 3% from the measured power consumption.

- observing the lifetime of the WSD and WSN network under the clustering protocol by using the new model. First, we compare our proposed model with the well-known analytic model presented in [23] and with a practical model dedicated to the low power media access (BMAC) analysis [13]. Then, we illustrate the impact of both the transition and the data transfer energy-costs.

The rest of this paper is organized as follows: Section II gives an overview of the different works on energy modelling available in the literature. Section III presents briefly the WSD hardware architecture, before providing a detailed investigation of the enhanced energy modelling. Section IV describes the different functional WSD elements and the experimental setup. The power consumption measurement assessment and the power profile identification of the different phases in the communication process are introduced in Section V. Section VI discusses the proposed energy model and the consumed energy by the interaction of different phases. Section VII presents a use case of our model in terms of WSD lifetime and cluster-based network lifetime. Conclusions and future research directions are provided in Section VIII.

II. ENERGY MODEL OVERVIEW

An essential requirement in optimizing the network lifetime is to understand how the system consumes energy. Some of the research works already developed the energy models and power measurements of WSDs. A common limitation of previous research is to study separately the MCU and radio parts (Table I). Much established energy models consider only the RM because it is assumed to be an energivore. Again, most of them do not integrate all different states of the RM and MCU that constitute the WSD. Moreover, the mutual interaction between these two parts is neglected.

TABLE I: Energy model parameters considered in various literature's

	MCU Parts				Radio Parts				Mutual	Usage classifications			
	AM	TRN	Sleep	Tx	Rx	Listen	Sleep	STR	TRN	TRF	Model	MAC	NET	Observation
[23]–[25]	-	-	-	√	√	-	-	-	-	-	Analytic	-	CL	NL
[26]	-	-	-	√	√	-	-	-	-	-	Analytic	-	CL	NR
[27]	-	-	-	√	√	-	-	-	-	-	Analytic	-	RT	NL
[28]	-	-	-	√	√	-	-	-	-	-	Analytic	-	RT	NRG
[29]	-	-	-	√	√	-	-	-	-	-	Analytic	√	RT	NL
[11]	-	-	-	√	√	-	-	-	-	-	Analytic	-	RT	NRG
[6], [7]	-	-	-	√	√	-	-	√	-	-	Analytic	√	-	RxTx
[8]	-	-	-	√	√	-	√	√	-	-	Analytic	-	-	Modem
[9]	-	-	-	√	√	-	-	√	√	-	Analytic	-	-	DL
[10]	-	-	-	√	√	-	-	-	-	-	Analytic	-	-	RxTx
[13]	-	-	-	√	√	√	√	-	-	-	Pratical	√	RT	NRG
[14]	-	-	-	√	√	-	√	-	√	-	Pratical	-	-	Conso
[15]	-	-	-	√	√	√	√	√	√	-	Pratical	√	-	Conso
[44], [45]	√	√	√	-	-	-	-	-	-	-	N/A	-	-	Conso
[46], [47]	√	-	√	√	√	√	√	-	-	-	Pratical	√	-	Conso
[3]	√	-	√	√	√	-	√	-	-	-	Pratical	√	-	DL
[49], [50]	√	-	√	√	√	-	√	√	-	-	Pratical	√	-	DL
Our work	√	√	√	√	√	√	√	√	√	√	Pratical	√	CL,RT	DL,NL

AM: Active Mode, TRN: Transition state, Tx: Transmission phase, Rx: reception phase, STR: Radio start-up stage, TRF: Data transfer phase,
CL: Clustering, RT: Routing protocol, NL/DL: Network/Device Lifetime, NR: Network Reliability, NRG: Energy-efficiency or saving,
RxTx: Radio design, N/A: Not Assessed, Modem: Modulator-Demodulator design, Conso: Power consumption

Based on the first radio energy model for WSNs proposed in [23], the authors observed the network lifetime performance considering the cluster-based network topology. This model was widely used for optimizing the network lifetime and reliability for cluster-based protocols [23]–[26] and flat routing protocols [27]. This model is also used for the energy optimization problem in routing protocol based on the genetic algorithm [28] and for the cross-layer optimization of correlated data collection [29]. However, this analytic model is limited as it is based on the assumption of an unlimited reliable Tx range. It only considers the Rx and Tx phases of the RM unit, in which, the Rx value is assumed to be constant and the Tx output power varies with the distance between the transmitter and the receiver. Other works have described the upper limit of the energy model based on an unlimited Tx range according to a distance [6]–[11]. They attempted to introduce models that individually incorporate the major components constituting the radio subsystem.

The work in [11] considers the effective Tx range. This is modelled by the PA output power of the transmitting, LNA sensitivity of the receiving module and the RF environment. The Rx power to receive data reliably is supposed to be a constant. Throughout this model, the authors highlighted the network energy performance by observing the multi-hop or single-hop routing protocol. The remaining work has focused on the design techniques to reduce the power consumption of the radio module [6]–[10]. Most of the works characterized the radio subsystem into three circuit blocks which include the baseband circuit (data encode/decode), the modem circuits and the PA output power. Based on this, the authors pointed out that RM circuit blocks must be designed according to the system-level across the entire network. Towards this end, the time-dependent energy model was expressed in terms of the power consumption of each circuit block during data com-

munication. Commonly, the radio model includes the effect of the power consumption of the Tx circuit (modulation), PA output transmit-power, Rx circuit (demodulation) and the modem start-up time [6]–[9]. Moreover, the Tx and Rx times are expressed as the packet size and the data rate ratio. It has been approved that the start-up time has a significant impact on the total energy consumption. The difference between these works lies in the detailed consideration of each component making up the radio circuit block. In [6], the additional power consumption for the Tx and Rx baseband circuits corresponds to the data encoding and decoding compared to the work in [7]. At the system level, energy-efficient modulation design techniques and MAC protocols have been observed from the standpoint of block's power consumption.

In [8], the energy-constrained modulation optimization strategy has been investigated to minimize the total energy consumption required to send a data-bit. Authors assumed that the radio works in multi-states mode: the active state, the sleep state and the start-up phase. During data Rx and Tx modes, all modem circuit elements work into the active state; when there is no data, they work in the sleep state; and when switching from sleep state to active state, there is a start-up phase. This operating mode allows significant energy savings when the sleep state is deployed. Correspondingly, the total energy consumption required to send data-bits also consists of these three components: power consumption values for the active mode, the sleep mode, and the start-up mode. The start-up duration is equal to the frequency synthesizer's settling time. The active mode power comprises the Tx power and the circuit block power. Specifically, the circuit power consumption consists of the mixer, the FS, the LNA, the active filter at the transmitter/receiver, the IFA, the DAC/ADC and the PA. The PA power depends on the PA drain efficiency and the peak-to-average ratio, which is dependent on the modulation

scheme and the associated constellation size. However, Tx power should be part of the total amplifier power consumption. The energy consumption in the baseband is supposed to be smaller and not considered in the calculations.

In [9], the authors described a simple energy model for wireless transceivers. They applied their model to observe the battery lifetime of the Bluetooth transceiver. The radio is supposed to have three operation modes: start-up, receive and transmit mode. Also, they incorporated a transient time between receive and transmit modes to allow for channel switching or to absorb any transient behaviour. The radio start-up consumption model is related to the time for the FS and the VCO to lock onto the carrier frequency. It has been noticed that FS and VCO are the elements which are shared between receiver and PA. Thus, Tx power consumption includes the FS, the VCO and the PA power consumption. The PA energy was based on the PA efficiency, data rate, transmission distance and path loss exponent. While, the Rx power consumption includes the power consumption of FS and VCO, the LNA, mixer and IFA power consumption. The IFA power is supposed to vary with the data rate. Throughout this model, they observed that the device lifetime has significantly improved as the data rate increases, the start-up time decreases, and the PA efficiency improves. However, the same author mentioned that the data rate does not scale with power consumption due to the fixed power consumption cost of the transmitter electronics [10]. Therefore, they have argued that the energy consumption model should depend on the features of the device architecture and its behaviour. They considered Tx power consumption based on the global power consumption of the transmit block and the PA power consumption. They developed a simple metric to evaluate the energy cost of both the communication protocol and circuit electronics. This metric treats the electronics energy as an overhead cost on top of the required SNR per bit for a given BER (Eb/No). The radio energy-efficiency was determined by the ratio between both the communication and the electronic circuit energy costs. However, they did not take into account the energy consumption at start-up, transient and sleep modes, even though their impact on the overall energy consumption of the radio has already been demonstrated.

These different analytical energy models only focus on the transceiver subsystem's energy modelling. Also, these models are limited to the Tx and Rx phases and the energy consumption in the subsystem circuit. The Tx power has been written with the PA parameter of the transmitter and RF environment. This method is often referred to as the variable power management strategy [15]. While, the subsystem circuit power consumption is often assumed constant, unless it is used in the context of modulation optimization to determine the optimal modem parameters for a LP transceiver design [5]–[8]. Practically, the power consumption in the transceiver circuit depends on the state in which the device operates. Many research works have reformulated energy consumption by taking the WSD operating mode states and total energy consumption, considering all transition states, instead of evaluating only for the steady states of the device [12]–[15].

In the versatile low power media access communication

(BMAC) for WSNs, the radio device is supposed to operate in four states, which are Tx, Rx, idle listening and sleeping states [13]. Also, there is consideration of data sampling time before each data transmission, which is assumed to be application based. This is expensive and affects the lifetime of the WSD, and its value is assumed to be 1100ms. For the design and energy model of BMAC protocol, the time duration and current consumption are taken from experimental measurement values of the Mica2 WSD [41] and the Chipcon CC1000 transceiver [51]. The BMAC's energy performance is observed with a multi-hop network. However, the energy consumption of the startup state and the transition between states are not integrated into this model. An extension of an energy model was developed for the Chipcon CC2420, an IEEE802.15.4 trade device [14]. This model is derived from the power consumption measurement in the four steady states i.e. power down, idle, Rx and Tx, and their related transitions. They defined that in the power down state, the voltage regulator is turned on, however, but the crystal oscillator is disabled. In the idle state, the voltage regulator and oscillator are on. Practically, these two low-power managements are a methodology for implementing the sleeping state [52]. They observed that the transitional energies have a significant impact on the total WSD power consumption.

Some researchers have attempted to address more realistic considerations. Authors in [15] proposed a realistic energy consumption model of the communication subsystem, which was derived from the measured power consumption performance of real WSDs, based on CC1000 [51] and CC2420 [52]. They defined six different states: Tx, Rx, listening, sleeping, idling and waking. Here, the sleeping state means a turn-off Radio, the idling state define as idling but not listening, while being aware of nothing will happen. The waking state corresponds to the start-up process from sleeping (off) mode to idling mode. Considering all the transitions, the authors were interested in observing the energy efficiency of WSN sleep scheduling protocols.

Furthermore, a realistic power consumption model for time-slot channel hopping (TSCH) networks was developed [46], [47]. Authors argued that in a typical WSD, the two components that consume the most energy are the MCU and the radio [46]. As the MCU and radio change state, their consumption varies. A TSCH schedule can contain different time slot types to indicate that a WSD should transmit, receive, listen or put its radio to sleep [47]. They supposed the MCU could work into two modes: sleep mode and active mode. While the radio must be able to operate in three states: Tx, Rx, Listening and sleep state [46], to which idling state is added in [47]. They experimentally observed the reliability of the suggested model by comparing the measured values of all time slots to their modelled counterpart. Then, these different CPU and radio states are taken into account in the comparison of device lifetime in wireless networks for the Internet of Things [3]. But no energy cost for transitions between states is added. On the other hand, the authors in [44], [45] investigated the MCU energy consumption by considering the active state, sleep state and its transitions. Some works have attempted to measure WSD power consumption and WSN energy consumption [41]–

[43]. MicaZ® power consumption has been investigated in [41] and an evaluation of Telos® power consumption is given in [42]. However, the authors did not provide a model.

In [49], the authors proposed an energy consumption model based on LoRa and LoRaWAN to estimate the consumed power of each LoRa device element. To study device autonomy, the analytical model considers the following three main device units: the sensor, the MCU and RM units. The authors in [40] proposed EMs which have been derived based on current consumption measurements on a currently prevalent LoRaWAN hardware platform. It allowed them to quantify the impact of relevant physical and Medium Access Control (MAC) layer LoRaWAN parameters and mechanisms, as well as Bit Error Rate (BER) and collisions, on energy performance. The same authors conducted a similar investigation with Sigfox hardware device [50]. In contrast, these works did not take into account the transition state energies, data transfers and listening energies in their EMs.

The work done in [6]–[15], [23] does not allow predicting WSD lifetime accurately, and also the work done in [3], [46]–[50] does not serve the purpose. None of them considers WSD activity modes under the data communication process. Thus, data transfer between the MCU and the RM is ignored in this model. For this reason, we believe that to improve the results previously obtained, the model should be described by a function of the WSD features. Thus, in this work, we derive the power consumption model from the structure and behaviour of the WSD during the communication process. In addition, we verify the results through measurements using TelosB [48]. Also, the WSD system energy modelling procedure provides a precise estimation of the energy consumption within each activity mode which is related to the data communication process, mainly during reception and transmission modes. Profiling the WSD energy consumption during its respective activity and operation modes further helps to manage the energy consumption efficiently according to the available energy and WSD requirements.

III. ENERGY MODELLING OF WSD SYSTEM

This section deals with the determination of the enhanced model of the energy consumption for WSDs, taking into account the communication process. The latter can be declined into Tx and Rx modes. These two modes will be characterized by different phases that can also be called states. First, the WSD hardware architecture will be presented briefly before entering the modelling phase. We consider a WSD architecture that enables monitoring the environmental phenomenon such as temperature and humidity and sends measured data to the base station (gateway) using a single or multi-hop network.

A. WSD Hardware Architecture

The WSD depicted in Fig. 1 can use its energy for sensing, MCU and RMs [23], [42]. The sensing module is a type of electronic sensor capable of detecting and measuring physical phenomena. The digital or analog output signals depend on selected sensors. The MCU module is responsible for collecting, processing and storing the output signal from
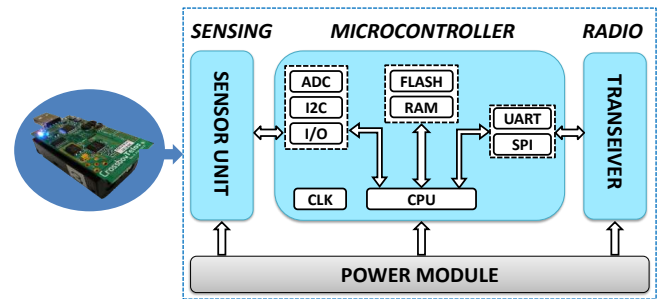

Fig. 1: Typical Architecture of WSD hardware

the sensing module. Furthermore, once the sensing data is stored, the MCU controls the RM and transfers the data and address packets to it. Then, the RM supports data transmission or reception to/from another WSD or a network gateway. Fig. 2 summarizes WSD operation phases and timing periods scheme.

B. WSD Energy Modelling

The energy model is based on the extraction of a relevant elements for the different modules regarding their energy cost. Fig. 2 shows a possible generic WSD operation scheme involving the WSD functional components, with their different states and associated time duration. The presented model focuses on the impact of the data size throughout the communication process. Thus, the model is based on the following assumptions:

- The sensing step is repeated several times with a determined repetition number and duration. For a deployment scenario, this energy quantity is generally constant, and it can be calculated with a suitable model [13], [53].
- The sensing data is already stored in the MCU Internal Memory (MIM), such as Flash or RAM memory.
- After data storing, the WSD will be in sleep mode until it communicates.
- Each WSD operation phase is defined by its time period and duration.
- The RM can be characterized by steady power consumption phases such as Tx, Rx and listening phase, as well as the switching between the different phases [6], [9].
- Finally, the MCU module can be also switched from the active state to the LPMs to save energy after performing the task [44], [54].

The datasheet of the different modules constituting the WSD provides the reference values about the operating voltage and the associated consumed current for the various steady states. It gives the power consumption of the whole WSD system. However, the operating times of each module are not provided. Moreover, each module is studied independently under different conditions. Thus, an appropriate energy model is needed.

Based on the observations from Fig. 2, we target a new approach. We would like to emphasize the energy signature associated with the mutual interaction of the different modules, especially, the mutual interaction between the MCU and
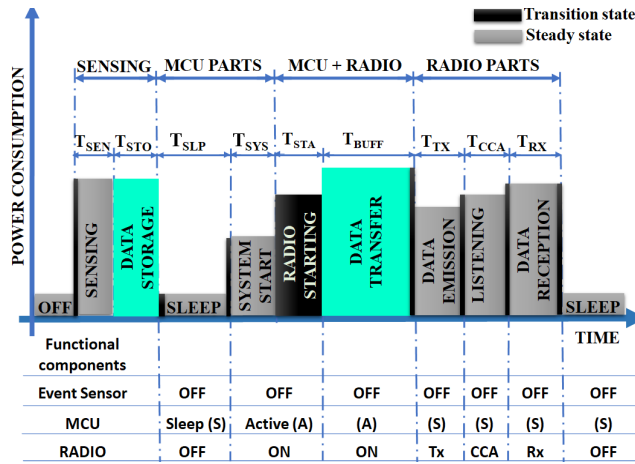
Fig. 2: WSD operation phases and timing periods scheme.

Radio modules. From our understanding, mutual data transfers should have a greater impact on the energy model which is generally not considered in the other models. Therefore, the modelling is elaborated on three main parts of WSD: MCU, MCU/Radio data exchange and Radio consumption in the following.

1) MCU Part Energy modelling: The MCU manages and controls the sleep and start-up mode of the radio module for data communication. Moreover, the MCU should remain asleep without any operation or peripheral control. Thus, it can operate commonly in three main states such as deep sleep (off), sleep and active state. Let us denote M^k as the set of the MCU main state, that is $M^k =\{$off, sleep, active$\}$, where k is the index of the main state family. Therefore, the energy consumed by the MCU into the main state M^k can be expressed as follows:

$$E_{mcu}^{(k)} = \sum_{k=1}^{n} P_{mcu}^{(k)} \times T_{mcu}^{(k)} \qquad (1)$$

where n is the state number and $P_{mcu}^{(k)}$ is the power consumed in the state (k). $T_{mcu}^{(k)}$ is defined as the time spent in this state.

The transition states energy, $E_{mcu}^{(k,i)}$ is expressed as:

$$E_{mcu}^{(k,i)} = \sum_{k=1,i\neq k}^{m} P_{mcu}^{(k,i)} \times T_{mcu}^{(k,i)} \qquad (2)$$
$$= \sum_{k=1,i\neq k}^{m} (P_{mcu}^{(k)} + P_{mcu}^{(i)}) \times \frac{T_{mcu}^{(k,i)}}{2}$$

where (k,i) denotes the index of state transition from two different main states and m the total number of the transition state. $P_{mcu}^{(k,i)}$ and $T_{mcu}^{(k,i)}$ are respectively the power and time required to perform the transition between two states (k,i).

According to Fig. 2, the time spent during the main state is composed of the period when the MCU remains in either sleep or active state which are $T_{mcu}^{(S)}$ or $T_{mcu}^{(A)}$, respectively. The MCU active state period is composed of the time duration for different phases which are the system start-up T_{SYS}, the radio starting T_{STA} and the data transfer T_{BUFF}. The latter can have different values for Tx and Rx, $T_{BUFF}^{(Tx)}$ for transmission

and $T_{BUFF}^{(Rx)}$ for reception phases. While, the MCU sleep period consists of the duration for which the WSD stays in sleep mode T_{SLP}, the time duration of the transmission T_{TX}, listening T_{CCA} and reception T_{RX} for the radio module. Thus, $T_{mcu}^{(S)}$ and $T_{mcu}^{(A)}$ can be expressed as:

$$T_{mcu}^{(S)} = T_{SLP} + T_{TX} + T_{CCA} + T_{RX} \qquad (3)$$
$$T_{mcu}^{(A)} = T_{SYS} + T_{STA} + T_{BUFF} \qquad (4)$$

Given the power consumed during the sleep state and active state which are $P_{mcu}^{(S)}$ and $P_{mcu}^{(A)}$, respectively, the expression (1) can be simplified as follows:

$$E_{mcu}^{(k)} = P_{mcu}^{(S)} \times T_{mcu}^{(S)} + P_{mcu}^{(A)} \times T_{mcu}^{(A)} \qquad (5)$$

$P_{mcu}^{(A)}$ depends on the Central Processing Unit (CPU) operating frequency. Its impact on the MCU power consumption will be presented according to the payload size (sub-section VI-A).

2) MCU and Radio Part Energy Modelling: Practically, the MCU sends an interrupt to start and configure the radio module for different transmit and receive modes [47], [55]. Then, the data stored in MIM must be transferred through the data FIFO of the MAC layer to the radio module buffer. The data transfer energy between MIM and Radio is composed of consumed energy for the radio start-up and data transfer energy during transmit and receive mode, denoted $E_{Radio}^{(STA)}$, $E_{mcu/Radio}^{(Tx)}$ and $E_{mcu/Radio}^{(Rx)}$, respectively. Conceptually, let's consider that the MCU and Radio module start independently, the energy during radio start-up can be described as:

$$E_{Radio}^{(STA)} = (P_{Radio}^{(ON)} + 2P_{mcu}^{(A)}) \times \frac{T_{STA}}{2} \qquad (6)$$

where $P_{mcu}^{(ON)}$ is the radio module power consumption in the radio ON state, and T_{STA} is the radio start-up time. It's noticed that the ON state power consumed can be referred at idle listening state (see for example Table VI).

For the transmit mode, data transfer energy consumption $E_{mcu/Radio}^{(Tx)}$ is the energy cost-per-bit of data transfer from MIM to the radio transmit buffer (TxFIFO). The Serial Peripheral Interface (SPI) ensures data transfer. Its hardware is made of a simple shift register characterized by its baud rate and transfer capacity [41], [42], [54]. Energy is a function of timing and power dissipated by data reading from the MIM and data writing into the SPI transmitter buffer (TxBUF). When TxBUF is ready, the data is sent to the TxFIFO before putting it in the transmission channel. At the TxFIFO, data can be written as a byte or a word at a time. The data reading time mainly depends on the capacity of the bus and the CPU frequency. The energy to transfer L-bits data can be determined as follows:

$$E_{mcu/Radio}^{(Tx)} = P_{mcu/Radio}^{(Tx)} \times T_{BUFF}^{(Tx)}. \qquad (7)$$

$T_{BUFF}^{(Tx)}$ is the Tx data transfer time duration expressed as:

$$T_{BUFF}^{(Tx)} = \frac{2L}{\lambda f_{sys}} + \frac{L+h_1}{\lambda B_r} + \frac{L_{Radio}^{Seg}}{\lambda B_r} + \frac{L+h_2}{\lambda B_r} \qquad (8)$$

where $f_{sys}, B_r, h_1, L_{Radio}^{Seg}, D_s, h_2$ and λ are system frequency, SPI baud rate, SPI header, TxFIFO segment size,

modulator symbol rate, radio packet header, and transfer capacity, respectively. $P_{mcu/Radio}^{(Tx)}$ is MCU and Radio power consumed during TxFIFO data transfer phase (Table VI).

However, for the receive mode, data transfer energy consumption $E_{mcu/Radio}^{Rx}$ is the energy cost-per-bit of data transfer from the radio receiver buffer (RxFIFO) to the MIM. The energy depends on the timing and the power dissipated by receiving the data via the transmission channel and writing it to the RxFIFO. When RxFIFO is ready, the data is sent to the SPI receiver buffer (RxBUF) before being stored in the MIM. At RxFIFO, one byte or one word of data can be read at each time. Let us consider the MIM to be of flash memory type, that is partitioned into segments or sectors. There is the smallest size of flash memory that can be erased before data writing [41], [42], [54]. Thus, the data storage time is deduced from the flash frequency-time generator, F_{tg}, during the erasing and writing operations. For RAM memory type, the flash frequency-time generator can be assimilated to the CPU operating frequency. The energy to transfer L-bits data can be determined as follows:

$$E_{mcu/Radio}^{(Rx)} = P_{mcu/Radio}^{(Rx)} \times T_{BUFF}^{(Rx)} \qquad (9)$$

$T_{BUFF}^{(Rx)}$ is the Rx data transfer time duration expressed as:

$$T_{BUFF}^{(Rx)} = \frac{L + h_2}{\lambda D_s} + \frac{L_{Radio}^{Seg}}{\lambda B_r} + \frac{L + h_1}{\lambda B_r} + \frac{L}{\lambda F_{tg}} + T_{rz} \quad (10)$$

where, T_{rz} is a segment erasing time. It is noted that this erasing time depends on the memory type and technology used. $P_{mcu/Radio}^{(Rx)}$ is MCU and Radio power consumed during RxFIFO data transfer (Table VI). Practically, B_r value should be synchronized with the clock frequency for writing and reading of slave module.

3) Radio Part Energy Modelling: The radio part energy consists of the energy cost per-bit during listening, transmission and reception states as well as their transition states. Indeed, listening energy $E_{Radio}^{(CCA)}$ depends on the channel access estimated time, T_{CCA}, which depends on the MAC protocol used, and the power consumption P_{Radio}^{CCA} radio equivalent to the listening phase. It can be expressed as:

$$E_{Radio}^{(CCA)} = P_{Radio}^{(CCA)} \times T_{CCA}. \qquad (11)$$

The transmission energy, E_{Radio}^{TX}, for transmitting a L-bit data with a symbol rate D_s, is calculated as:

$$E_{Radio}^{(Tx)} = P_{Radio}^{(Tx)} \frac{L + h_2}{D_s} \qquad (12)$$

while the energy consumed to receive this L-bit data is expressed as:

$$E_{Radio}^{(Rx)} = P_{Radio}^{(Rx)} \frac{L + h_2}{D_s} \qquad (13)$$

The radio transition states energy can be deduced as follows:

$$E_{Radio}^{(k,i)} = \sum_{k=1, i \neq k}^{m} P_{Radio}^{(k,i)} \times T_{Radio}^{(k,i)} \qquad (14)$$

$$= \sum_{k=1, i \neq k}^{m} (P_{Radio}^{(k)} + P_{Radio}^{(i)}) \times \frac{T_{Radio}^{(k,i)}}{2}$$
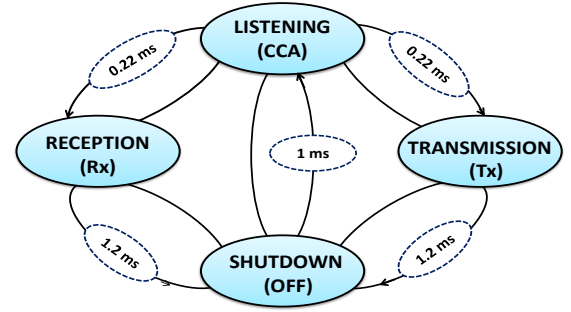

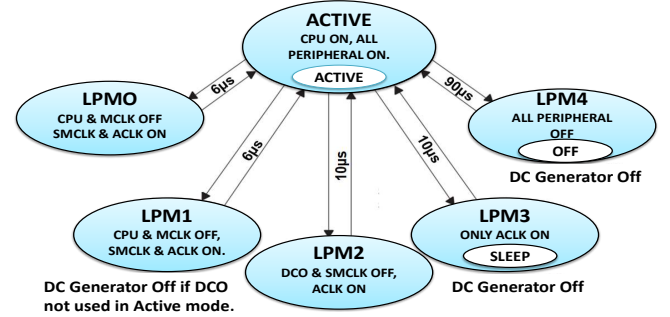Fig. 3: CC2420 State and Transition Diagram [52]

Fig. 4: MCU inter-mode and its transition time duration [54]

where $P_{Radio}^{(i)}$ is the power consumed in the state (i), $T_{Radio}^{(i)}$ is the time spent in this state. $P_{Radio}^{(k,i)}$, $T_{Radio}^{(k,i)}$ are the power and time for the transitions between two states (k, i). m is the transition state total number.

The next section describe succinctly the experimental setup and telosB device with its possible interacting states, used for the experiments.

IV. EXPERIMENTAL INVESTIGATION ON TELOSB

In this section, the TelosB WSD description will be presented by outlining its different internal phases in the communication process. In fact, it is important to examine the hardware interaction sections to see how much energy each one requires. Thus, we will explore the experimental setup for real-time power consumption analysis.

A. TelosB WSD Description and its interacting states.

In this experimental setup, the considered WSD is TelosB. It is composed of the Chipcon CC2420 transceiver and the TI-MSP430 16-bit microcontroller [48]. MSP430 has two internal memories of $10kB$ RAM and $48kB$ of flash memory. It also has two independently configurable internal timers [54]. The Timer module is frequently used, to trigger an event or to issue an interrupt to other external modules such as the Transceiver. The CC2420 transceiver is controlled by the MSP430 via SPI bus as well as by a series of I/O and interrupts lines. The MCU can be used to put out the CC2420 if necessary. The TelosB operates with the operating system TinyOS.

Fig. 3 illustrates the steady states of the CC2420 which are Tx, Rx, Listen and Off states [52]. Through our measurement results, it is important to underline that the transition between
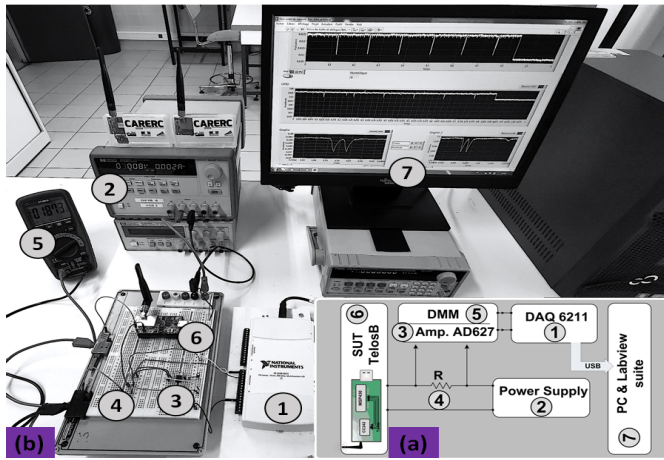
This article has been accepted for publication in IEEE Sensors Journal. This is the author's version which has not been fully edited and content may change prior to final publication. Citation information: DOI 10.1109/JSEN.2022.3212933

8   IEEE SENSORS JOURNAL, VOL. XX, NO. XX, XXXX 2017

Fig. 5: Experimental setup (a) synoptic and (b) photo.

TABLE II: Experimental setup parameters and settings

N°	Tools	Parameters	Symbol	Values
1	DAQ NI 6211	Sampling rate	$\mathcal{R}_s$	50 kHz
2	Agilent E3632A	Voltage supply	$\mathcal{V}$	3 V
3	AD627	Amplifier gain	G	10 and 100
4	Resistor $\frac{1}{4}$ W, E24	Shunt resistance	R	12 Ω
5	DMM FI 122, 10 A			
6	Telos			

states is affected by undesirable delay latencies varying from a hundred microseconds to some milliseconds. While, TI-MSP430 MCU supports the dynamic power management mechanism to properly manage its energy consumption and avoid a permanent stay in the Active mode (AM). MSP430 can be operated at various Low Power Modes (LPM) which can be selected via software. An interrupt event can wake up MSP430 from one of the five LPMs, respond to the request, and return to the LPM when the interrupt program finishes. Fig. 4 depicts the inter-mode timing of the MSP430 with the transition delay according to the MSP430 datasheet [54]. This process includes the considered Off, Active and Sleep states.

B. Experimental Setup of TelosB Device

To observe the consumed energy of the TelosB device, in this work, we use three tools and their compromises during the profiling process such as a digital multimeter (DMM FI 122) which is optional, a voltage supply generator Agilent E3632A and a digital acquisition system NI Labview, DAQ 6211. The advantages of this measuring equipment are the high input impedance of the DAQ, that is, the negligible influence of the DAQ on the operation of the system, the facilitation of processing and storing data, and finally the automation possibility of the power profiling process, i.e. splitting of each phase, with the Labview software. Moreover, the instruments are portable, lightweight and mobile. Table II lists the elements of the experimental setup and their related parameter values. Fig. 5 shows the experimental set-up developed for the TelosB device. The power measurement will be done by connecting the shunt resistor insertion between the System Under Test telosB (SUTB) and the voltage generator. For measurement

reliability, the low noise PA instrumentation AD627 circuit output is connected to a digital voltmeter to check the voltage across this circuit at any time, which is optional. The amplified output voltage signal was also sampled with a DAQ NI6211 with a sampling rate of $\mathcal{R}_s = 50kHz$. The shunt resistance value R used for acquiring the SUTB current is 12Ω. The stabilized voltage supply is defined as $\mathcal{V} = 3V$. Temperature in the measurement laboratory is 20°C.

The instantaneous potential difference across the resistor is $\nu_r(t)$, which is connected to the inputs of the instrumentation amplifier (AD627), with a gain G=10 and G=100 for measuring the current of the order of milliamperes and microamperes, respectively. The current value flowing through the SUTB is obtained by the ohm's law: $i(t) = \nu_r(t)/R$, and the effective voltage applied on the SUTB is: $\nu_s = \mathcal{V} - \nu_r(t)$. Thus, the experimental power consumption model can be determined at each instant t by the following expression:

$$\mathcal{P}_M^{(\cdot)}(t) = \nu_s \times \frac{i(t)}{G} = (\mathcal{V} - \nu_r(t)) \times \frac{\nu_r(t)}{R} \times \frac{1}{G} \qquad (15)$$

The energy consumed $E_M^{(\cdot)}(t_1, t_2)$ during time interval $[t_1; t_2]$ can be calculated as:

$$E_M^{(\cdot)}(t_1, t_2) = \int_{t_1}^{t_2} \mathcal{P}_M^{(\cdot)}(t) dt \qquad (16)$$

The energy consumed approximately over N samples is obtained by using the trapezoid rule of numerical integration method provided by Labview software.

In the next section, we present the experimental validation of the model based on the power profile of each the WSD components.

V. EXPERIMENTAL RESULTS AND EVALUATION

The present section discusses the estimated power consumed by MCU module, radio module and the data transfer (MCU/Radio) phase during the communication process. Before that, we present the measurement evaluation of each LPM consumption for MSP430. The approaches adopted follow the pseudo-code presented in Table III.

A. MCU Part Current Consumption

As previously mentioned, MSP430 has five different LPM states according to the current configuration of its clock system [54]. It operates with the following modes: the clock is activated for Active mode and the CPU becomes disabled in LPM_0. Then, the LPM_1 disabled the DCO oscillator for the fast master clock (MCLK), while LPM_2 disabled the fast slave clock (SMCLK). DC generator is disabled for LPM_3, while the crystal oscillator for the auxiliary clock (ACLK) is disabled for LPM_4. The measurement evaluation of each LPM mode is made independently, and at each measurement, the adopted approach is to disable all components, interrupts and peripherals. Then, define the desired frequency and the CPU power mode, lock the system operation and record the respective measurements (Table IIIa). The following two tables present the average values of 50 different result measurements. These are used to verify the model precision by comparing the

This article has been accepted for publication in IEEE Sensors Journal. This is the author's version which has not been fully edited and content may change prior to final publication. Citation information: DOI 10.1109/JSEN.2022.3212933

AUTHOR *et al.*: PREPARATION OF PAPERS FOR IEEE TRANSACTIONS AND JOURNALS (FEBRUARY 2017)   9

TABLE III: Measuring methodologies pseudo-codes.

(a) MCU measuring	(c) Radio Tx measuring
CPU_setProfile(frequency){	OnSystem_booted(){
Disable_All_Peripherals( );	Disable_All_Peripherals( );
Disable_All_Interrupts( );	Disable_All_Interrupts( );
CPU_setPowerMode(xx);	CPU.setClock(frequency);
CPU_setClock(frequency);	RADIO_setPower(Tx);
// Here the system is locked	TIMER_startPeriodic(temps);
// Start Measurements	}
}	event TimerHandler.fired(){
(b) Radio Rx measuring	done=false;
OnSystem_booted(){	RADIO_startingUp();
Disable_All_Peripherals( );	DATA_TRANSFER_start(pld);
Disable_All_Interrupts( );	RADIO_startSend (pld);
CPU.setClock(frequency);	while(!done)
RADIO_startingUp();	CPU_setPowerMode(LPM3);
}	}
event Radio.receive(message){	event RadioHandler.sendDone(){
DATA_TRANSFER_start(pld);	done=true;
CPU_setPowerMode(LPM3);	RADIO_stop();
}	}

Fig. 6: The power consumption of WSD under communication process: (a) Tx mode and (b) Rx mode.

TABLE IV: MCU Current Consumed (f_{sys}=1 MHz,3 V)

Power	Measured Current (μA)			Datasheet (μA)	
	Max	Mean	Min	Max	Min
Active	543.6	512.5	479.1	600	500
LPM_0	81.6	76.9	75.8	n/a	n/a
LPM_1	79.8	76.1	75.5	n/a	n/a
LPM_2	18.9	17.8	17.6	n/a	n/a
LPM_3	3.16	2.98	2.88	3	2.6
LPM_4	0.54	0.50	0.43	n/a	n/a

measured values with the TelosB datasheet values [48]. The consumed currents in different LPM_{0-4} modes are shown in Table V and IV. In the sleep state, TelosB operates in mode LPM_3. Then, we see a consumption reduction, it's about 11 times between the active mode and LPM_{0-1}, and about 4.5 to 5 times between LPM_{0-1} and LPM_{2-3-4}. Moreover, the current requirement of the system which operates in $1MHz$ frequency is approximately 4 times smaller than $4MHz$. The MCU remains in the sleep state and switches only to the active state to perform some tasks for energy saving. Then, energy consumption depends on the time spent in different states.

B. Communication Process Different Phases Identification

Fig. 2 and Fig. 6 illustrate the WSD operating sequence. The pseudo-code shown in Table III.a, describes the measurement

TABLE V: MCU Current Consumed (f_{sys}=4 MHz,3 V)

Power	Measured Current (μA)			Datasheet (μA)	
	Max	Mean	Min	Max	Min
Active	2180	2050	1902	2400	1800
LPM_0	340.6	320.3	297.2	n/a	n/a
LPM_1	317.9	312	311.2	n/a	n/a
LPM_2	70.1	68.1	68	n/a	n/a
LPM_3	60.5	56.9	54.3	n/a	n/a
LPM_4	13.6	12.7	11.8	21	5.1

process. After the data sensing and storage procedure is done, the WSD switches to sleep mode (LMP_3) until the timer will be fired. Then, the MCU switches to the active state and initializes the radio configuration. Upon radio's crystal oscillator (RCO) stabilization [52], the MCU also sends an access command to the Rx/Tx-FIFO in order to transfer all information about addresses and data through the SPI. When the buffering is completed, the MCU returns to LPM_3 mode and the radio switches to idle listening. After a backoff time delay and two contention windows for channel clear assessment, as soon as the channel is free, the WSD switches to the Tx phase. Immediately after the Tx phase, WSD goes to sleep state i.e only the MCU operates in LPM_3 mode. In Receive mode, the process is reversed after WSD start-up. Fig. 6 is briefly composed of the following elementary parts:

- WSD starts in sleep mode. After timer interrupt, the radio wake-up phase begins (wait for RCO stabilization),
- Followed by the data transfer phase,
- The Listening phase which is composed of backoff delay and two contention windows in Tx mode,
- The Tx or Rx phase takes place. Finally, radio stopping process occurs.

The Tx process consumption measurement is investigated by varying transmission power and data size. While the Rx process can be only evaluated according to the data size. The WSD sends periodically a fixed-size packet per second. The data packet is constituted of headers and data. The power consumption measurement of the Tx and Rx process is performed independently with two different TelosB. This procedure is repeated 50 times. Fig. 6 shows the power consumption of WSD during the Tx and Rx communication process with the signal sampling frequency as $50kHz$, data size L= $50bytes$ and the transmit power Tx= $0dBm$. The other parameters described below are chosen according to the datasheet recommendation and user's guide of CC2420 and MSP430: f_{SYS}= $4MHz$, B_r= $256kbps$, h_1= $3bytes$, L_{Radio}^{Seg}= $128bytes$, D_s= $250kbps$, h_2= $11bytes$, λ= $1byte$, F_{ftg}= f_{SYS} with T_{rz}= $360\mu s$.

TABLE VI: CC2420 Average Current Consumed, Tx (dBm)

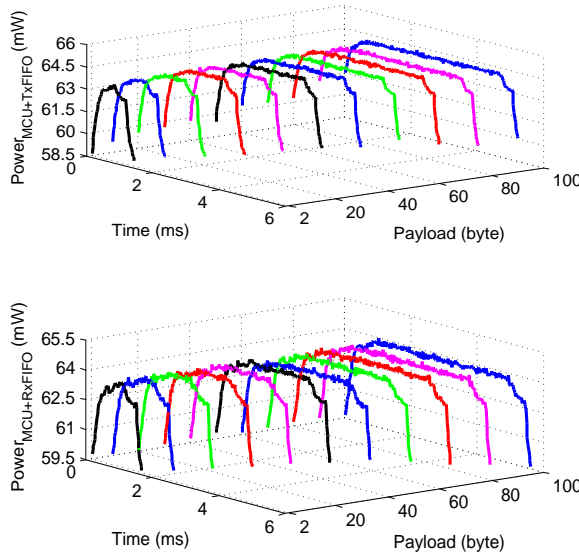| Mode		Measured Current (mA)				Datasheet Telos (mA)		
		MCU/Radio		Radio		MCU/Radio		Radio
		Min	Max	Min	Max	Min	Max	
Tx	0	21	21.2	17.5	18.5	19.5	21	17.4
	-1	18.8	19.4	16.7	17.1	n/a	n/a	16.5
	-3	17.9	18.5	15.5	16.5	n/a	n/a	15.2
	-5	16.5	17.2	13.9	14.3	n/a	n/a	13.8
	-7	15.2	15.9	12.5	13.3	n/a	n/a	12.5
	-10	13.9	14.5	11.2	11.8	n/a	n/a	11.2
	-15	12.6	13.2	10	10.9	n/a	n/a	9.9
	-25	11.2	11.89	8.55	9.53	n/a	n/a	8.5
Rx		21	21.	18.8	18.9	21.8	23	19.7
Listening		x	x	19.8	20.1	x	x	n/a

Fig. 7: The power consumption of data transfer: (a) MIM to TxFIFO phase and (b) RxFIFO to MIM phase.

C. Rx Power Consumption Versus Tx Signal Power

Measurement results are shown in Table VI by comparing with the values provided by the TelosB datasheet [48]. Through these results, the listening phase consumes much more power than the Tx or Rx phases because the MCU stays into LPM_3 in order to react quickly to the initial signals. Moreover, the current consumed by the listening state of transmitting and reception has a small difference, $19.8mA$ and $20.1mA$ respectively, due to the electronic circuit difference used by the receiver and transmitter. Furthermore, the MCU/Radio column corresponds to the current consumption of the data transfer phase from the MIM into the RxTx-FIFO, this phase is obviously a power consumer. It is because the MCU and the Radio run in the active state simultaneously until the data in the MIM is transferred completely to the RxTx-FIFO. This phase duration is quantified in terms of the SPI transfer rate and the time spent to read or write the MIM and RxTx-FIFO as we see in relations (7) and (9).

As illustrated in Fig. 7, the Tx and Rx data transfer duration phases depend on the data packet size to be communicated. Table VI indicates that the current required for Tx phase
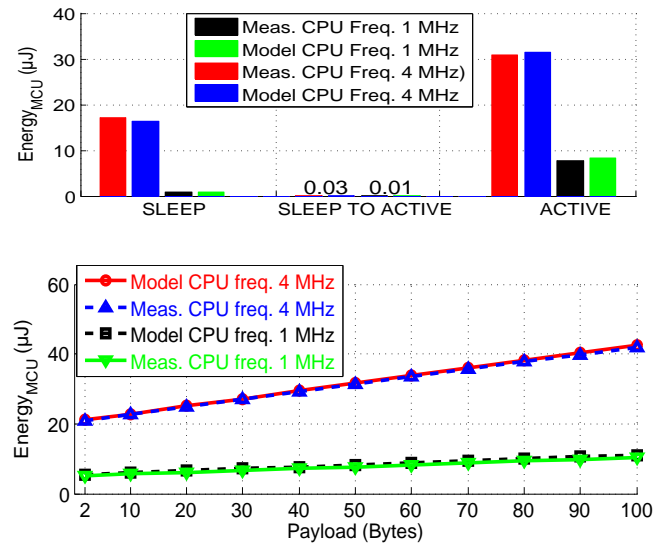

Fig. 8: MSP430 Energy consumption (a) Transition mode, (b) Active Mode

consumption varies according to the Tx power.

VI. MODEL VALIDATION AND DISCUSSION

The present section discusses the proposed energy model and the estimated energy consumed by each module during the communication process according to Fig. 6. The results from the model are obtained using the different relations discussed in section (III-B) combined with the power values provided in the datasheet. While the measurement results are obtained by performing a numerical integration trapezoidal rule provided by Virtual Instrumentation (Vi)'s Labview software.

A. MCU Energy Measurement and Model Results

Relations (5) and (2) allow determination of the MSP430 energy consumption model. The MCU remains in the sleep state and switches only to AM state in order to perform some tasks for energy saving. Then, energy consumption depends on the time spent in the different LPM states. In our scheme, the system remains in sleep mode for $100ms$ before the timer starts. Then, the TinyOS scheduler switches automatically the MSP430 into the sleep state. Next, the MCU switches to AM state in order to control the radio start-up until the data packet is transmitted to the TxFIFO. Thus, the MSP430 active time duration also depends on the radio start-up period, and the payload size to be transmitted. These values can be found in Fig. 3 and Fig. 4 and relation (7), respectively. Fig. 8 illustrates the energy consumption comparison in sleep, transition and active modes referring to the MCU operating frequency and the energy consumption evolution according to the payload size. The transient energy from sleep to active is negligible with a value of $0.03\mu J$.

The energy-efficiency provided by MCU operating at $1MHz$ frequency is clearly shown in Fig. 8a. We can see that it is reduced by 66% compared to $4MHz$ CPU frequency. Besides, from Fig. 8b we can see that the energy model is closely
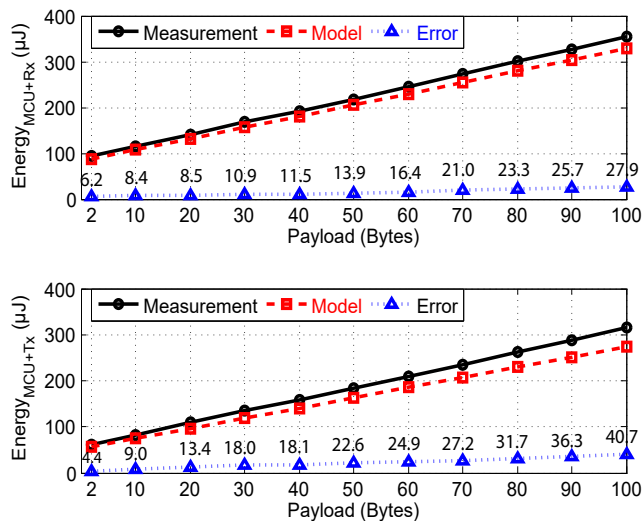
Fig. 9: Energy consumed by data transfer (a) MIM to TxFIFO and (b) RxFIFO to MIM.

matching with the measurements. The energy consumption evolves linearly as the payload size increases. We noticed that staying in sleep mode for $100ms$ consumes energy of $17.07\mu J$ while sending a data payload of $20bytes$. For a payload of $50bytes$ consumption is approximately $24.8\mu J$ and $31.2\mu J$. Thus, the value is increased by 1.5 and 1.8 times, respectively, compared to sleep mode. This means that the time duration plays a very important role in energy consumption. Thus, the compromise between active and sleep timing must be taken into consideration to play optimally with the MSP430 energy according to the amount of delivered data payload.

B. Data transfer Energy Measurement and Model Results

Relations (7) and (9) allow to find out the data transfer phases energy consumption model. According to Fig. 6, the data transfer is supposed to be started right after the radio start-up. The starting energy is calculated from relation (6) which gives a theoretical value of $16.2\mu J$ with time duration as $0.5ms$ (Fig. 3), and its measured value is $18\mu J$. Fig. 9 illustrates the energy consumption comparison data transfer from MIM to TxFIFO (MIM2TxF) and RxFIFO to MIM (Rx2MIM). We can also see that the energy consumption model and measurement increase linearly according to the data payload size. Thus, if the data payload size increases, power consumption also increases. This essentially confirms that the MIM2TxF and RxF2MIM data transfer duration is related to the data transfer rate and the system operating frequency. However, there is a small error that we can observe between the model and the measurement results, which also grows according to the data payload size. Observing the Fig. 3, using a data payload size 20 and $50bytes$, the average energy consumption for MIM2TxF data transfer are respectively $108\mu J$ and $184\mu J$. Accordingly, Rx2MIM data transfer is respectively $141\mu J$ and $218\ \mu J$. That means the Rx2MIM data transfer consumes more energy than MIM2TxF. This is

the fact that the Rx2MIM data transfer is synchronized with the modulator symbol rate and the delay of memory writing timing. We can report that in Tx2MIM mode, the relative error between the theoretical model and the experimental model (based on the measurement) from 2 to $100bytes$ is about 6% to 8%. Whereas in Rx2MIM mode, the relative error slightly increases linearly between 5.5% and 6%. We have these results because the commands strobe reading or writing are never made instantly. This is due to the need for access time required to perform operations. A minimum time delay between the instant the command is sent and the instant when the actual data is accessed (reading or writing the data). However, it is sometimes also necessary to take into account a cycle time greater than the access time by adding the memory cycle. That is in fact, the minimum time interval between two successive accesses. Otherwise, the duration of data processing can also generate energy consumption, which depends on the MCU system frequency, the instruction numbers and the program counter timing to the memory address access. Thus, this requires the number and the different instruction types used as well as the clock period per instruction. We did not consider these different periods, because they are all different for each memory type and MCU architecture. One of our objectives is to have an experimental acceptable energy model that allows us to evaluate the energy consumption of a communication process according to the system parameters available in the user's manual of different modules.

C. Radio Energy Measurement and Model Results

Relations (11), (12) and (13) allow to determine the energy consumption model of the different steady phases for the radio module. Through Fig. 6, the reception and transmission phase could be started after the channel listening phase. The CC2420 radio stack provides a clear channel assessment (CCA) before attempting to transmit. Tinyos had implemented CSMA/CA protocol which runs by default if no other protocol is specified. According to the CSMA algorithm, the channel listening phase ensures that the channel is clear for two contention window (CW) duration before transmitting. The CW is related to the timing interval between two successive CCA probes [52, p.53]. Before that, the channel listening period is delayed by a random delay chosen uniformly between 0 and 2^{BE}, where BE is the backoff exponent, to reduce the collision probability [13], [16], [17]. In our experimental results, the listening period varies in the range of $1.6ms$ to $5.6ms$, which corresponds to the energy consumption of $98.9\mu J$ and $333.6\mu J$, respectively. On data reception, let us suppose that the WSD receiver start-up was synchronized with the WSD transmitter and the data propagation duration is negligible. Besides, the transition from listening to transmission (CCA2Tx) or reception (CCA2Rx) is not instantaneous due to the use of different hardware. CC2420 transceiver itself provides a command strobe for transiting to the Tx state if the channel is currently clear after two contention window time duration. The transition duration is around $0.22ms$, and the CCA2Tx transition energy cost is about $12.30\mu J$ and $11.48\mu J$ for the energy model and the measurement, respectively. Whereas, the CCA2Rx transition
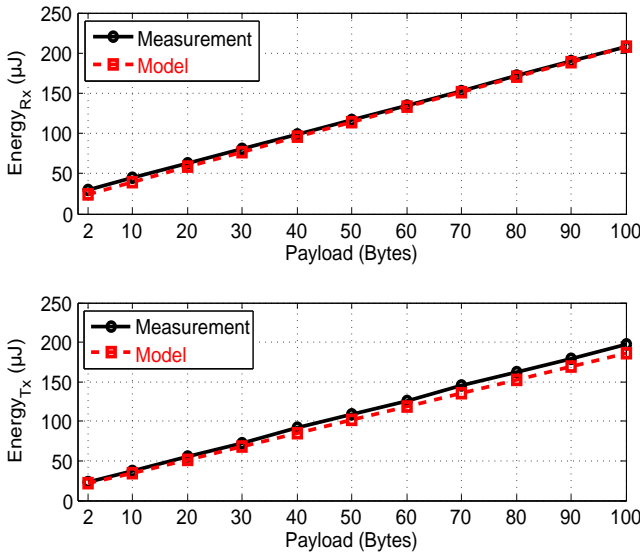
This article has been accepted for publication in IEEE Sensors Journal. This is the author's version which has not been fully edited and content may change prior to final publication. Citation information: DOI 10.1109/JSEN.2022.3212933

12

IEEE SENSORS JOURNAL, VOL. XX, NO. XX, XXXX 2017

Fig. 10: Energy consumed: (a) Tx phase and (b) Rx phase.

TABLE VII: WSD Energy consumed summaries (μJ), L=50 Bytes, Tx=0 dBm

Energy	Timer	STA	MCU	RxTx	TFR	TRN	CCA
Meas.	18.5	18	48.3	225.5	402	84.0	216.3
Model	n/a	16.2	48.2	224.1	370	84.2	216.3

Fig. 11: WSD Energy consumption statistical under communication.

energy cost is about $13.12\mu J$ and $12.35\mu J$ for the energy model and the measurement, respectively. It is seen that the model is increased by 6% over the measurement results. This is due to the fact that the CCA2Tx and CCA2Rx transitions did not evolve linearly. Let us deduce that it remains appropriate to minimize the impact of the various errors previously noted with respect to the global model. The results shown in Fig. 10 present the Rx and Tx phases energy consumption model and the experience according to the data payload size. The results show that the energy model is closely matching with the measurements. Then, the energy grows linearly, as the size of the data packet increases, the energy consumption also increases. This essentially confirms that the Rx/Tx duration period of a data packet depends on the modulator symbol rate. The results show that as the data payload size 20 and $50 bytes$, the average energy consumption for the Tx phase are respectively $54.9\mu J$ and $108.4\mu J$, whereas the Rx phase is $62.8\mu J$ and $117.1\mu J$, respectively. Thus, the Rx phase energy consumption is greater than that of the Tx phase. Finally, the time duration for going into the sleep state is approximately $1.2\ ms$ with a consumed energy of $26.1\mu J$ and $27.65\mu J$ for the energy model and the measurement, respectively.

D. Average Energy Assessment

In order to estimate the influence of each phase on the overall WSD consumption. Table VII summaries the different consumption of each different relevant element during communication process. In this result, the consumption of the timer and the radio initialization energy for stabilizing crystal oscillator (STA) is respectively $18.5\mu J$ and $18\mu J$ which represent 3% of WSD overall energy consumption.

The different phases in the RM consume much more energy than the MCU module. The energy consumed by the timer to initiate the start-up is about 8 times less than that of the RM, while the MCU consumption is approximately 5.5 times less than that of the RM. MCU consumption represents 5% of Telos

overall energy consumption. Thereby, by studying the communication process: the data transmission and reception (RxTx) consume 22% of the WSD total energy, which is distributed 10.5% and 11.5% for Tx and Rx, respectively. For the CC2420 transceiver, the data Rx consumes more energy than data Tx, which is contrary to the generic model proposed in [23]. Then, the channel access assessment (CCA) also represents 22% of the WSD total energy consumption. Furthermore, by analyzing data transfers, it has a very important energy cost both in MIM2TxF and RxF2MIM with associated consumption up to 18% to 22%, respectively. As shown in Fig. 11, this energy transfer represents 40% of global WSD consumption.

VII. ENERGY MODEL USE CASES

This section presents an example of a use case for our energy model. Firstly, it determine the WSD lifetime when WSD sends or receives a data packet. Then, we also apply this model to evaluate cluster-based routing protocol in term of network lifetime.

A. Use case: WSD lifetime comparison

The model energy expressions developed in the section III allow us to determine the entire WSD energy consumption during TX mode, $E_{WSD}^{(Tx)}$, as:

$$E_{WSD}^{(Tx)} = \sum_{k=1}^{m} P_{mcu}^{(k)} T_{mcu}^{(k)} + \sum_{k=1, i\neq k}^{m} P_{mcu}^{(k,i)} T_{mcu}^{(k,i)}$$
$$+ \sum_{z=1}^{m} P_{radio}^{(z)} T_{radio}^{(z)} + \sum_{z=1, j\neq z}^{m} P_{radio}^{(z,j)} T_{radio}^{(z,j)}$$
$$+ E_{mcu/Radio}^{(Tx)} \qquad (17)$$

It is recalled that k and z are the index of steady state family, for the MCU module there are three main states $M^k = \{$ *off, sleep, active* $\}$. While for the radio module, there are $M^z = \{$ *off, listen, transmission, reception* $\}$.

TABLE VIII: WSD lifetime comparison

	Previous works				Our works			
	[23]		[13]		Model		Meas.	
Period	Rx	Tx	Rx	Tx	Rx	Tx	Rx	Tx
1 s	3.94	10.44	1.04	1.02	0.61	0.57	0.57	0.54
1 mn	19.02	20.07	15.58	15.50	6.13	6.06	6.06	5.99
5 mn	20.10	20.32	19.20	19.18	6.99	6.97	6.97	6.95
15 mn	20.29	20.36	19.97	19.96	7.16	7.15	7.15	7.14
30 mn	20.34	20.37	20.18	20.17	7.20	7.19	7.19	7.19
1 hour	20.36	20.38	20.28	20.27	7.22	7.22	7.22	7.21
1 day	20.38	20.38	20.37	20.37	7.24	7.24	7.24	7.24

Let us assume that the receiver and transmitter start synchronously, the entire WSD energy consumption during RX mode, $E_{WSD}^{(Rx)}$, can be determined as:

$$E_{WSD}^{(Rx)} = \sum_{k=1}^{m} P_{mcu}^{(k)} T_{mcu}^{(k)} + \sum_{k=1,i\neq k}^{m} P_{mcu}^{(k,i)} T_{mcu}^{(k,i)}$$
$$+ \sum_{k=1}^{m} P_{radio}^{(k)} T_{radio}^{(k)} + \sum_{k=1,i\neq k}^{m} P_{radio}^{(k,i)} T_{radio}^{(k,i)}$$
$$+ E_{mcu/Radio}^{(Rx)} \qquad (18)$$

To determine the WSD lifetime, we consider two AAA batteries with a capacity $Q = 1250mAh$ and its voltage $E = 1.5V$ with leakage current $I_{lq} = 7uA$. These parameters give us the nominal energy $E_o = 13.5kJ$, and the leakage energy $E_{lq} = 21\mu J$. The battery autonomy, T_{bat}, is dependent on the total energy consumed and its capacity, which can be found as follow:

$$T_{bat} = \frac{E_o}{E_{lq}} \qquad (19)$$

This relation gives us $T_{bat} = 20.39 \ years$ approximately.

Analogously, the WSD lifetime can be bounded by the available energy. Thus, it can be found throughout the relation (19) by replacing the battery leakage energy by the WSD energy consumed.

To complete the comparative study between the analytic-based model and our model, we consider Friis free space propagation model [56]. In which, the received signal power is expressed a function of distance between the transmitter and the receiver as:

$$P_{Rx} = P_{Tx} \times \frac{\lambda^2 G_{Tx} G_{Rx}}{(4\pi)^2 L_s d^\alpha} \qquad (20)$$

P_{Rx} is the RX signal power, d is a separation distance between the transmitter and the receiver, P_{Tx} is the TX signal power, G_{Tx} and G_{Rx} are the gains of transmitter and receiver antennas, λ is the wavelength of carrier. L_s represents other system losses that is not associated with the propagation loss. The parameter α is the path-loss exponent which takes constant values depending on the environment. In [23], $\alpha = 2$ and $\alpha = 4$ are considered for free-space and multi-path model respectively. In this work, the antenna gain parameters $G_{Tx} = 2dBi$ and $G_{Rx} = 2dBi$, the TX power $P_{Tx} = 0dBm$, the receiver sensitivity $P_{Rx} = -78dBm$, and telosB transmission frequency is $2.45GHz$. From relation (20), we can calculate the distance d, which is $130m$ approximately.

Table VIII shows the WSD lifetime comparison depending on data sampling period. It illustrates the comparison results of EMs developed for LEACH [23], BMAC [13] and our works in terms of the device lifetime estimation. It is clearly shown that our model outperforms LEACH and BMAC EMs. We can also see that the WSD lifetime increases remarkably according to the data sampling period.

Regarding our work, if the data sampling period is defined as 1 second and if the WSD is in RX mode, the WSD lifetime estimation of our model and measurement can reach approximately 0.61 year and 0.57 year, respectively. There is an 6.4% error between the model and the measurement. While, the WSD is in TX mode, the WSD lifetime estimation of our model and measurement can reach approximately 0.57 year and 0.54 year respectively, there is 6% error observed. If the data sampling period is defined as 5 minutes and the WSD is in RX mode, the WSD lifetime estimation of our model and measurement can reach approximately 6.99 years and 6.97 years, respectively. There is an 0.26% error between the model and the measurement. While, the WSD is in TX mode, the WSD lifetime prediction of our model and measurement can reach approximately 6.97 years and 6.95 years respectively, there is 0.25% error observed. Thus, it can be seen that when the period increases the error decreases significantly.

Moreover, As the data sampling period is greater than 5 minutes, we can see that the lifetime estimation of WSD under our model is approximately improved by 3 times compared to LEACH and BMAC EMs. The reason is that our EM considers all transitions states and mutual data transfers between MCU and RM. For example, if the data sampling period is defined as 15 minutes and if the WSD is in TX mode, our EM reaches approximately 7.15 years, whereas LEACH and BMAC EMs can reach 20.36 years and 19.96 years respectively. The WSD lifetime estimation of our model is 64.69% and 64.35% greater than LEACH and BMAC EMs respectively.

B. Network lifetimes

In our previous work, our research was oriented towards cluster-based network organization which is an important approach for meeting the energy-efficiency objective through energy balance [24], [25]. LEACH concept is to divide the network operation into a round time which requires two main operation: cluster heads (CHs) selection and assignment of each WSD to one cluster [23], [24]. Each WSD has the same probability of becoming a CH. The task of being a CH is rotated between WSDs according to a round time. The decisions are based on a threshold function $p_i(r)$ for CH election. All WSDs generate a random number between [0 1]. If it is less than a threshold $p_i(r)$, the WSD becomes CH during the current round r. The threshold is defined as:

$$p_n(r) = \begin{cases} \frac{k}{n-k*(r\,mod\,\frac{N}{k})} & \text{if } n \in G \\ 0 & \text{otherwise} \end{cases} \qquad (21)$$

where n and k are the number of WSDs and CHs in the network, G is the set of WSDs that have not been CHs in the last N/k rounds.
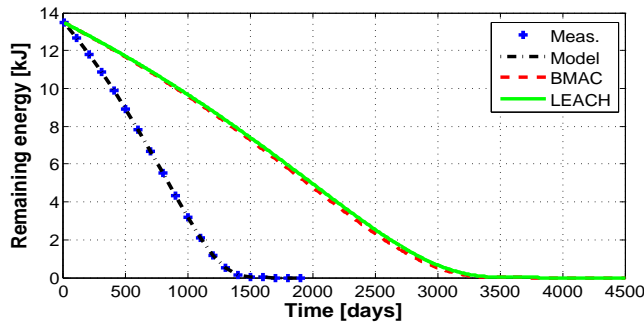
Fig. 12: Network lifetime

In order to evaluate the network lifetime, let us consider that there exist $n = 100$ WSDs distributed randomly in $100m \times 100m$ area. Lifetime may be computed for a discrete set of values at round time r that depends on the network application [53]. We have considered a clustered-based network in which $k = 5$ cluster at every round time r can be ensured [25]. Each CH dissipates its energy for receiving data from member WSDs, aggregating the data, and transmitting the aggregated data to the Base Station (BS). Therefore, the energy dissipated from the CH during a round can be expressed as:

$$E_{CH}(n, k) = (\frac{n}{k} - 1)E_{WSD}^{(Rx)} + E_{WSD}^{(Tx)} \tag{22}$$

Where, E_{TX} and E_{RX} are the total energy consumption of the WSD during transmit and receive modes, respectively. Thus, the energy consumed by each WSD cluster member to transmit the sensed data to its "CH" can be expressed as:

$$E_{nonCH} = E_{WSD}^{(Tx)} \tag{23}$$

And, the energy dissipated in a cluster per round, $E_{CL}(r)$, can be expressed as:

$$E_{CL}(r) = E_{CH} + (\frac{n}{k} - 1)E_{nonCH} \tag{24}$$

We can deduce the total energy dissipated in the network at each time round, E_{round}, which can be expressed as:

$$E_{round} = k \cdot E_{CL} \tag{25}$$

To have a comparative study between the analytic-based model and our model, we consider the same parameters described in VII-A. Moreover, the TX power inside the cluster is defined at $P_{Tx} = -7dBm$ with threshold distance $d = 70m$, CH TX power is $P_{Tx} = 0dBm$ and the round time is $r = 15$ minutes.

Figure 12 shows the evolution of network remaining energy as a function of time (days). We can see that the average remaining energy estimation of a WSD under our EM is obviously greater than the LEACH and BMAC models. In term of the network lifetime, our model's estimation is approximately improved by 2.3 times compared to LEACH and BMAC EMs. For example, our EM reaches approximately 1613 days (4.42 years), whereas LEACH and BMAC EMs can reach 3808 days and 3738 days (10.43 and 10.24 years) respectively. Thus, our model exhibits 57.62% and 56.82% better lifetime estimation

over LEACH and BMAC EMs, respectively. Furthermore, if we consider relation (23), defining a direct communication between the WSD and the BS with TX power $P_{Tx} = 0dBm$, the WSD lifetime can reach 7.15 years whereas network lifetime can only reach 4.42 years. The reason is that our EM takes into account a mutual data transfer between MCU and RM. Thus, the CHs expend their energy quickly because they compute data aggregation before data forwarding to the BS.

VIII. CONCLUSION

The energy modelling based on power consumption measurement of WSN during the communication process is investigated. We have seen that power profile measurements can provide deep knowledge of energy consumption for different phases of the WSD operation. In this paper, we proposed an accurate model which takes into account the different stages of transmission and reception communication modes. The analytical expressions of the developed model were given as a function of the data packet lengths, data rate, operation status and the predesigned stages versus appropriate communication bus and power mode. The WSD energy model was validated with measurement results. Results show that the data transfer phase between the MCU and the RM is one of the major energy consumers representing up to 40% of total energy consumed. The experimental validation demonstrates that the model accuracy for all payload sizes from 2-to-100 bytes and the calculated power consumption differs on average by less than 3% from the measured power consumption. This study may allow software designers for developing suitable energy-aware communication protocols and can help the hardware designers for choosing a communication bus, the different modules used, and estimate the WSD lifetime.

The proposed energy model can be practically adopted for different types of wireless devices for the Internet of Things [3]. An energy-optimization opportunistic spectrum access algorithm for LoRa object is under study. It will be interesting to study the optimal good-put depending on data packet length for lifetime maximization [2], which can be a future research direction.

REFERENCES

[1] H. Yetgin, K. T. K. Cheung, M. El-Hajjar, and L. H. Hanzo, "A survey of network lifetime maximization techniques in wireless sensor networks," *IEEE Communications Surveys & Tutorials*, vol. 19, no. 2, pp. 828–854, 2017.

[2] F. Engmann, F. A. Katsriku, J.-D. Abdulai, K. S. Adu-Manu, and F. K. Banaseka, "Prolonging the lifetime of wireless sensor networks: A review of current techniques," *Wireless Communications and Mobile Computing*, vol. 2018, pp. 1–23, 2018.

[3] E. Morin, M. Maman, R. Guizzetti, and A. Duda, "Comparison of the device lifetime in wireless networks for the internet of things," *IEEE Access*, vol. 5, pp. 7097–7114, 2017.

[4] F. Karray, M. W. Jmal, A. Garcia-Ortiz, M. Abid, and A. M. Obeid, "A comprehensive survey on wireless sensor node hardware platforms," *Computer Networks*, vol. 144, pp. 89 – 110, 2018.

[5] O. Kanoun, S. Bradai, S. Khriji, G. Bouattour, D. El Houssaini, M. Ben Ammar, S. Naifar, A. Bouhamed, F. Derbel, and C. Viehweger, "Energy-aware system design for autonomous wireless sensor nodes: A comprehensive review," *Sensors*, vol. 21, no. 2, p. 548, 2021.

[6] E. Shih, S. Cho, F. S. Lee, B. H. Calhoun, and A. Chandrakasan, "Design considerations for energy-efficient radios in wireless microsensor networks," *VLSI signal processing systems for signal, image and video technology*, vol. 37, pp. 77–94, 2004.

[7] A. Wang, S. Cho, C. Sodini, and A. Chandrakasan, "Energy efficient modulation and mac for asymmetric rf microsensor systems," in *Proceedings of the 2001 international symposium on Low power electronics and design*, 2001, pp. 106–111.

[8] S. Cui, A. J. Goldsmith, and A. Bahai, "Energy-constrained modulation optimization," *IEEE transactions on wireless communications*, vol. 4, no. 5, pp. 2349–2360, 2005.

[9] A. Y. Wang and C. G. Sodini, "A simple energy model for wireless microsensor transceivers," in *IEEE Global Telecommunications Conference, 2004. GLOBECOM '04.*, vol. 5, 2004, pp. 3205–3209 Vol.5.

[10] A. Y. Wang and C. G. Sodini, "On the energy efficiency of wireless transceivers," in *2006 IEEE International Conference on Communications*, vol. 8. IEEE, 2006, pp. 3783–3788.

[11] Q. Wang, M. Hempstead, and W. Yang, "A realistic power consumption model for wireless sensor network devices," in *2006 3rd Annual IEEE Communications Society on Sensor and Ad Hoc Communications and Networks*, vol. 1, 2006, pp. 286–295.

[12] G. Terrasson, R. Briand, S. Basrour, and V. Dupe, "A top-down approach for the design of low-power microsensor nodes for wireless sensor network," in *2009 Forum on Specification & Design Languages (FDL)*. IEEE, 2009, pp. 1–6.

[13] J. Polastre, J. Hill, and D. Culler, "Versatile low power media access for wireless sensor networks," in *Proceedings of the 2nd International Conference on Embedded Networked Sensor Systems*, ser. SenSys 04. New York, NY, USA: Association for Computing Machinery, 2004, pp. 95–107.

[14] I. Howitt, R. Neto, J. Wang, and J. M. Conrad, "Extended energy model for the low rate wpan," in *IEEE International Conference on Mobile Adhoc and Sensor Systems Conference, 2005.* IEEE, 2005, pp. 8–pp.

[15] Q. Wang and W. Yang, "Energy consumption model for power management in wireless sensor networks," in *2007 4th Annual IEEE Communications Society Conference on Sensor, Mesh and Ad Hoc Communications and Networks*. IEEE, 2007, pp. 142–151.

[16] G. M. Shafiullah, S. A. Azad, and A. B. M. S. Ali, "Energy-efficient wireless mac protocols for railway monitoring applications," *IEEE Transactions on Intelligent Transportation Systems*, vol. 14, no. 2, pp. 649–659, 2013.

[17] F. Z. Djiroun and D. Djenouri, "Mac protocols with wake-up radio for wireless sensor networks: A review," *IEEE Communications Surveys Tutorials*, vol. 19, no. 1, pp. 587–618, 2017.

[18] M. R. Ahmad, E. Dutkiewicz, and X. Huang, "A survey of low duty cycle mac protocols in wireless sensor networks," *InTech Emerging Communications for Wireless Sensor Networks*, p. 69, 2011.

[19] F. Alfayez, M. Hammoudeh, and A. Abuarqoub, "A survey on mac protocols for duty-cycled wireless sensor networks," *Procedia Computer Science*, vol. 73, pp. 482–489, 2015.

[20] M. Z. Hasan and F. Al-Turjman, "Evaluation of a duty-cycled asynchronous x-mac protocol for vehicular sensor networks," *EURASIP Journal on Wireless Communications and Networking*, vol. 2017, no. 1, pp. 1–16, 2017.

[21] Y. Zhang and W. W. Li, "Energy consumption analysis of a duty cycle wireless sensor network model," *IEEE Access*, vol. 7, pp. 33 405–33 413, 2019.

[22] A. Kozlowski and J. Sosnowski, "Energy efficiency trade-off between duty-cycling and wake-up radio techniques in iot networks," *Wireless Personal Communications volume*, vol. 107, pp. 1951–1971, 2019.

[23] W. B. Heinzelman, A. P. Chandrakasan, and H. Balakrishnan, "An application-specific protocol architecture for wireless microsensor networks," *IEEE Transactions on wireless communication*, vol. 1, no. 4, pp. 660 – 670, October 2002.

[24] R. Randriatsiferana, R. Lorion, F. Alicalapa, and F. Harivelo, "Energy-efficient clustering algorithm based on energy variance for wireless sensor networks," in *2013 International Conference on Smart Communications in Network Technologies (SaCoNeT)*, vol. 01, 2013, pp. 1–5.

[25] R. Randriatsiferana, H. T. C. Antilahy, F. Alicalapa, and R. Lorion, "Weighted route selection in cluster-based protocol forwireless sensor networks," *EAI Endorsed Transactions on Future Internet*, vol. 3, no. 8, 5 2016.

[26] I. Ez-Zazi, M. Arioua, A. El Oualkadi, and P. Lorenz, "On the performance of adaptive coding schemes for energy efficient and reliable clustered wireless sensor networks," *Ad Hoc Networks*, vol. 64, pp. 99–111, 2017.

[27] J.-H. Chang and L. Tassiulas, "Maximum lifetime routing in wireless sensor networks," *IEEE/ACM Transactions on networking*, vol. 12, no. 4, pp. 609–619, 2004.

[28] S. K. Jha and E. M. Eyong, "An energy optimization in wireless sensor networks by using genetic algorithm," *Telecommunication Systems*, vol. 67, no. 1, pp. 113–121, 2018.

[29] S. He, J. Chen, D. K. Yau, and Y. Sun, "Cross-layer optimization of correlated data gathering in wireless sensor networks," *IEEE Transactions on Mobile Computing*, vol. 11, no. 11, pp. 1678–1691, 2012.

[30] F. Fanian and M. K. Rafsanjani, "Cluster-based routing protocols in wireless sensor networks: A survey based on methodology," *Journal of Network and Computer Applications*, vol. 142, pp. 111 – 142, 2019.

[31] C. Nakas, D. Kandris, and G. Visvardis, "Energy efficient routing in wireless sensor networks: A comprehensive survey," *Algorithms*, vol. 13, no. 3, p. 72, Mar 2020.

[32] M. Younis and K. Akkaya, "Strategies and techniques for node placement in wireless sensor networks: A survey," *Ad Hoc Networks*, vol. 6, no. 4, pp. 621–655, 2008.

[33] H. Asharioun, H. Asadollahi, T.-C. Wan, and N. Gharaei, "A survey on analytical modeling and mitigation techniques for the energy hole problem in corona-based wireless sensor network," *Wireless Personal Communications*, vol. 81, no. 1, pp. 161–187, 2015.

[34] N. Sharmin, A. Karmaker, W. L. Lambert, M. S. Alam, and M. S. A. Shawkat, "Minimizing the energy hole problem in wireless sensor networks: A wedge merging approach," *Sensors*, vol. 20, no. 1, p. 277, Jan 2020.

[35] X. Huan, K. S. Kim, S. Lee, E. G. Lim, and A. Marshall, "A beaconless asymmetric energy-efficient time synchronization scheme for resource-constrained multi-hop wireless sensor networks," *IEEE Transactions on Communications*, vol. 68, no. 3, pp. 1716–1730, 2020.

[36] M. O. Farooq and T. Kunz, "Operating systems for wireless sensor networks: A survey," *Sensors*, vol. 11, no. 6, pp. 5900–5930, May 2011.

[37] O. Hahm, E. Baccelli, H. Petersen, and N. Tsiftes, "Operating systems for low-end devices in the internet of things: a survey," *IEEE Internet of Things Journal*, vol. 3, no. 5, pp. 720–734, 2015.

[38] A. Abuarqoub, M. Hammoudeh, F. Alfayez, and O. Aldabbas, "A survey on wireless sensor networks simulation tools and testbeds," *Sensors, transducers, signal condi-tioning and wireless sensors networks advances in sensors: reviews*, vol. 3, no. 14, pp. 283–302, 2016.

[39] Y. B. Zikria, H. Yu, M. K. Afzal, M. H. Rehmani, and O. Hahm, "Internet of things (iot): Operating system, applications and protocols design, and validation techniques," *Future Generation Computer Systems*, vol. 88, pp. 699–706, 2018.

[40] L. Casals, B. Mir, R. Vidal, and C. Gomez, "Modeling the energy performance of lorawan," *Sensors*, vol. 17, no. 10, p. 2364, 2017.

[41] L. Barboni and M. Valle, "Experimental analysis of wireless sensor nodes current consumption," in *2008 Second International Conference on Sensor Technologies and Applications (sensorcomm 2008)*, 2008, pp. 401–406.

[42] A. Prayati, C. Antonopoulos, T. Stoyanova, C. Koulamas, and G. Papadopoulos, "A modeling approach on the telosb wsn platform power consumption," *Journal of Systems and Software*, vol. 83, no. 8, pp. 1355–1363, 2010.

[43] C. Haas, J. Wilke, and V. Stöhr, "Realistic simulation of energy consumption in wireless sensor networks," in *European Conference on Wireless Sensor Networks*. Springer, 2012, pp. 82–97.

[44] K. Mikhaylov and J. Tervonen, "Optimization of microcontroller hardware parameters for wireless sensor network node power consumption and lifetime improvement," in *International Congress on Ultra Modern Telecommunications and Control Systems*, 2010, pp. 1150–1156.

[45] L. Chen, J. Warner, P. L. Yung, D. Zhou, W. Heinzelman, I. Demirkol, U. Muncuk, K. Chowdhury, and S. Basagni, "Reach2-mote: A range-extending passive wake-up wireless sensor node," *ACM Trans. Sen. Netw.*, vol. 11, no. 4, Dec. 2015.

[46] X. Vilajosana, Q. Wang, F. Chraim, T. Watteyne, T. Chang, and K. S. J. Pister, "A realistic energy consumption model for tsch networks," *IEEE Sensors Journal*, vol. 14, no. 2, pp. 482–489, 2014.

[47] G. Daneels, E. Municio, B. Van de Velde, G. Ergeerts, M. Weyn, S. Latré, and J. Famaey, "Accurate energy consumption modeling of ieee 802.15. 4e tsch using dual-bandopenmote hardware," *Sensors*, vol. 18, no. 2, p. 437, 2018.

[48] J. Polastre, R. Szewczyk, and D. Culler, "Telos: enabling ultra-low power wireless research," in *IPSN 2005. Fourth International Symposium on Information Processing in Sensor Networks, 2005.*, 2005, pp. 364–369.

[49] T. Bouguera, J.-F. Diouris, J.-J. Chaillout, R. Jaouadi, and G. Andrieux, "Energy consumption model for sensor nodes based on lora and lorawan," *Sensors*, vol. 18, no. 7, p. 2104, 2018.

[50] C. Gomez, J. C. Veras, R. Vidal, L. Casals, and J. Paradells, "A sigfox energy consumption model," *Sensors*, vol. 19, no. 3, p. 681, 2019.

[51] *CC1000 Data Sheet*. [Online]. Available: https://www.ti.com/lit/ds/symlink/cc1000.pdf

[52] *CC2420 Data Sheet*. [Online]. Available: https://www.ti.com/product/CC2420

[53] A. Mainwaring, D. Culler, J. Polastre, R. Szewczyk, and J. Anderson, "Wireless sensor networks for habitat monitoring," in *Proceedings of the 1st ACM International Workshop on Wireless Sensor Networks and Applications*, ser. WSNA 02. New York, NY, USA: Association for Computing Machinery, 2002, pp. 88–97.

[54] *MSP430x1xx Family: User's Guide*, 2006.

[55] A. J. Odey and D. Li, "Low power transceiver design parameters for wireless sensor networks," *Wireless Sensor Network*, vol. 4, pp. 243–249, 2012.

[56] S. K. Islam and M. R. Haider, *Sensors and low power signal processing*. Springer Science & Business Media, 2009.

Rivo RANDRIATSIFERANA received the Engineering degree in industrial computer science and electronic from the École Supérieure Polytechnique d'Antsiranana, Madagascar, in 2009, and the Ph.D. degree in networks and telecommunications from the University of Reunion, Reunion Island, France, in 2014. From 2014 to 2015, he was an assistant lecturer in teaching and research (ATER) at the University of La Reunion. Actually, He is associate professor at the University of Rennes 1, where he has been teaching in ISTIC syllabus since 2021 and associate researcher at IETR entity of CNRS (UMR 6164), Rennes. His research interests include energy optimization of wireless communication protocol, IoT and advanced application of the network tensor analysis for smart objects.

Frederic Alicalapa received his MSc in Electrical and Electronic Engineering in 1998, University of Bordeaux 1, IMS Lab, France. He received the Ph.D. degree in electronic analog IC design at the University of Bordeaux 1 (IMS Lab), on the Study and realization of controlled RF active inductances, using 0.8um silicon current conveyor circuit. His doctoral research concerns tunable filters, and tunable active inductance for RF circuits. He is currently an associate professor at the University of Reunion, France, and at the Energy Lab (LE2P). His research interests include the development of energy harvesting circuits, charge pump structures, wireless sensor networks, CMOS integrated circuits. He was involved in many local, national and european projects (REAVOLC, WSN Indian Ocean Cooperation, FEDER CARERC 1&2, STIC ASIA). He is involved in DETECT european project. He has held academic and administrative positions : Service on higher education committees (CNU 63, 2011-2015), Deputy Director of Physics Department (2013-2014), Director of Physics Department (2016-2018, 2018-2020).

Richard Lorion received his PhD in Physical Engineering (genetic algorithm) in 2000 from the University of Reunion, France. He was also head of Department of Data Communications and Computer Networks at Institute of Technology, University of La Reunion, France. He is currently an Associate Professor and Director of Institute of Technology at the University of Reunion, France. His research has been done since 2000 at the Energy Lab (LE2P), where he focuses on wireless network and wireless sensor networks, mobile computing and digital communication, protocols with emphases on energy-efficient routing algorithm and application.

Lala Rajaoarisoa received the M.Sc. and Ph.D. degree in automatic and computer sciences from the University of Aix-Marseille, Marseille, France, in 2005 and 2009, respectively. He is currently an Assistant Professor with the Institut Mines-Télécom Nord Europe. Develop predictive models and controllers to assess system behaviour and optimize its performance. This development includes the analysis of intrinsic properties such as stability, observability, identifiability, and controllability. He is involved in research activities dedicated to the optimization of energy efficiency of cyber-physical systems with more than 80 papers published in refereed journals and conferences. He regularly participates and contributes on several international projects (ANR, FUI, and INTERREG) and was the supervisor of more than of 15 Ph.D. students, postdocs, research engineers, and Master internships. His research interests include the development of data-driven tools and methods for the observation and control of large-scale distributed systems.

Blaise Ravelo is currently a University Full Professor at NUIST, Nanjing, China. His research interests include multiphysics and electronics engineering. He lectures on circuit and system theory, science, technology, engineering and maths (STEM), and applied physics. He is a pioneer of the negative group delay (NGD) concept about $t<0$ signal traveling in physical space. This extraordinary concept is potentially useful for anticipating and prediction all kind of information. He was the Research Director of 11 Ph.D. students (10 defended), postdoctorals, research engineers, and master internships. With U.S., Chinese, Indian, European, and African partners, he is actively involved and contributes on several international research projects (ANR, FUI, FP7, INTERREG, H2020, Euripides2, and Eurostars). He is a member of Electronics Letters (IET)'s Editorial Board as a Circuit and System Subject Editor. He is a member of the Scientific Technical Committee of Advanced Electromagnetic Symposium (AES), in 2013, and IMOC2021. He is ranked in Top 2% world's scientists (2020–2021) by Stanford University, USA. He has Google Scholar H-index (2022) = 26 and i10-index (2022) = 83. He is a member of research groups such as IEEE, URSI, GDR Ondes, and Radio Society, and (co)authors of more than 370 scientific research papers in new technologies published in international conference and journals. He is regularly invited to review papers submitted for publication to international journals (IEEE Transactions on Microwave Theory and Techniques, IEEE Transactions on Circuits and Systems, IEEE Transactions on Electromagnetic Compatibility, IEEE Transactions on Industrial Electronics, IEEE Access, IET CDS, and IET MAP) and books (Wiley and Intech Science).

Christophe Moy received the Eng., M.Sc., and Ph.D. degrees in electronics from the INSA of Rennes, France, in 1995 and 1999, respectively. He then worked for six years in Mitsubishi Electric ITE focused on software radio systems and concepts. He was a Professor with Supelec from 2005 to 2014, and with CentraleSupélec from 2015 to 2017. Actually, He is a Professor with the University of Rennes 1, where he has been teaching in ISTIC syllabus since 2017. His research has been done since 2005 in IETR entity of CNRS (UMR 6164) where he focuses on software radio, cognitive radio (learning for dynamic spectrum access, application for the Internet of Things) and green radio. He was involved in many European and French collaborative projects: NoE NEWCOM and NEWCOM++, E^2R, EULER, E^2R-phase2, A3S, Mopcom, Idromel, WiNoCoD, SoftRF, CominLabs TEPN.